Journal of Cleaner Production 414 (2023) 137723

Contents lists available at ScienceDirect

Journal of Cleaner Production

journal homepage: www.elsevier.com/locate/jclepro

Investigation of nanofluids in alkaline electrolytes: Stability, electrical properties, and hydrogen production

Shihao Wei [a], Boris V. Balakin [b], Pawel Kosinski [a,*]

[a] University of Bergen, Department of Physics and Technology, Bergen, Norway
[b] Western Norway University of Applied Sciences, Department of Mechanical and Marine Engineering, Bergen, Norway

ARTICLE INFO

Handling Editor: Panos Seferlis

Keywords:
Electrolysis
Carbon black
Nanofluids
Hydrogen production
Electrical properties

ABSTRACT

Utilizing solar energy efficiently and manufacturing hydrogen economically are the primary goals in the energy industry. In this paper, we present a novel method to solve both issues by exploiting the electrolysis of electrolyte-based nanofluids under the illumination of solar light. The carbon black nanoparticles/sodium hydroxide solution mixture of electrolyte nanofluids were prepared, which were then electrolyzed in a Hoffman voltameter to produce hydrogen. The results showed the hydrogen production rate improved by 23.62% when carbon black was used in the electrolyte. The optimal carbon black concentration was 0.04% or 0.2% depending on the experimental set-up used. Finally, a theoretical model was built to evaluate the total hydrogen production, which showed a good agreement with the experimental results when the carbon black concentration was lower than 0.1 wt%.

1. Introduction

Hydrogen is a renewable energy resource that promotes clean production as its combustion product is only water, ensuring sustainable consumption. Although hydrogen is a principal element in nature, most of it that can be used in power engineering needs to be manufactured. Currently, more than 90% of commercially used hydrogen is produced from fossil fuels (Rausch et al., 2014), leading to the emission of greenhouse gases during the production process. A promising way to produce hydrogen in a sustainable way is through water splitting reactions (Léon, 2008), which requires significant energy. This process can utilize the energy generated from renewable energy sources to produce high-purity hydrogen (Stamenkovic et al., 2017). However, the energy cost to harness hydrogen is higher than the total energy that is converted into hydrogen formation. Nowadays, the widely used technologies in water splitting reactions include water electrolysis, photovoltaic technique, photocatalytic water splitting, etc. (Godula-Jopek, 2015).

Water electrolysis is a technique that converts electricity into hydrogen, similar to the photovoltaic technique that utilizes electricity generated by photovoltaic cells to produce hydrogen (El-Emam and Özcan, 2019). When the electrolysis is conducted at low temperature (lower than 100 °C), three commonly used technologies are alkaline water electrolysis, proton exchange membrane water electrolysis, and anion exchange membrane water electrolysis (Li et al., 2022). The utilization of an exchange membrane enables the attainment of higher purity hydrogen. Nevertheless, this comes at the expense of increased costs, and these technologies have limited durability and a small stack scale (Buttler and Spliethoff, 2018; Grigoriev et al.,. 2020). Alkaline water electrolysis, as a more mature technology, offers low capital costs, relatively stable operation, and the ability to be scaled up to large capacities. However, it still faces the challenge of low efficiency (David et al., 2019). Therefore, to enhance efficiency, various methods can be employed to accelerate reaction kinetics and reduce voltage inputs, such as utilizing electrocatalysts, increasing temperature, increasing pressure, etc. (Lohmann-Richters et al., 2021).

Photocatalytic water splitting is a technique that utilizes photocatalysts to convert solar energy into hydrogen. However, despite clean and endless energy resources, photocatalysts face challenges such as high cost, low quantum yield, issues with excessive charge recombination, and limited light absorption capabilities (Sudhaik et al., 2018). Carbon-based nanomaterials are considered a promising option for photocatalysts (Kundu et al., 2020). These nanomaterials exhibit exceptional physicochemical properties, such as high thermal and chemical stability, large surface area, and improved electrical, mechanical, and optical properties (Rasool et al., 2023).

Moreover, another essential property of these carbon-based

* Corresponding author.
E-mail addresses: Shihao.wei@uib.no (S. Wei), Boris.Balakin@hvl.no (B.V. Balakin), pawel.kosinski@uib.no (P. Kosinski).

https://doi.org/10.1016/j.jclepro.2023.137723
Received 24 March 2023; Received in revised form 26 May 2023; Accepted 4 June 2023
Available online 5 June 2023

nanomaterials that has not received enough attention is electrical or thermoelectrical properties (Sheikholeslami and Bhatti, 2017). These materials consist of nanosized carbon-based particles that, when uniformly dispersed in a solvent, form nanofluids. One important thermoelectrical property is the enhanced heat transfer performance observed in nanofluids subjected to an applied electrical field or magnetic field (Wang et al., 2020). This critical discovery appealed to researchers who shifted study priority from thermal convection to thermomagnetic convection (Khan et al., 2016a,b; Khan et al., 2016a,b). Another paramount electrical property is electrical conductivity. It was experimentally studied on different nanoparticle-based nanofluids (Zawrah et al., 2016; Bagheli et al., 2015), and an improved Maxwell model was developed to estimate the electrical conductivity of water-based nanofluids (Minea, 2019).

Therefore, these exceptional electrical properties of carbon-based nanofluids make them an ideal electrolyte. According to Kim and Park (2021), carbon-based nanoparticles enhance electron and mass transfers at the active region interface in the electrolytes. Besides, other types of nanofluids also have been investigated. Liu et al. (2016) used aluminum nanoparticles and ferro/ferricyanide solution to produce electrolyte nanofluids (ENF). Their research demonstrated the potential thermogalvanic application of ENF by highlighting the enhenced mass transfer, electrical conductivity, and thermal conductivity observed. Another proposed application involves the use of ENF inside batteries. Wang and Wang (2016) investigated the performance of aluminum oxide-based nanofluids as a battery electrolyte. The results showed that aluminum oxide ENF could effectively improve the battery output and heat transfer due to electrochemical reactions within the ENF. Both proposed applications of ENF heavily rely on the stability of the nanofluids, which leads to a loss of effectiveness over time. In addition, they were limited to one-time use, determined by the concentration of aluminum ions posing harm to the environment.

However, currently, there is no widespread use of carbon-based nanofluids as a replacement for conventional electrolytes in water electrolysis. In (Hiraki et al., 2005), the authors dispersed waste aluminum dross with the size of 180–425 μm in a sodium hydroxide (SH) solution and tested the hydrogen production. The results showed that initial temperature significantly affected the reaction rate, and that using micro-sized aluminum-SH solution as an electrolyte only required 2% energy consumption and emitted 4% carbon dioxide compared to conventional methods to generate hydrogen. They owed this unexpected energy consumption to the aluminum dross. The micro-sized aluminum increased the total surface area in the solution, making the reaction faster. However, they pay more attention to the composition of aluminum hydroxide (another electrolysis product) in the study instead of how aluminum particles affected the electrolysis production. This study indicated that using ENF in producing hydrogen by water electrolysis and solar light irradiation can increase total hydrogen production.

First, the improved electrolysis efficiency requires a higher temperature, which can be achieved through the enhanced thermal properties of nanofluids when subjected to solar irradiation. Secondly, the nanoparticle motion in the electrolyte can promote electrolysis due to the electrical double layer (EDL). Thirdly, the applied electric field can enhance the convective heat transfer within nanofluids. To our knowledge, these factors were considered by only a few researchers, making it a completely new research field. As an example, we cite the work by Choi and Lee (2020), who reported a promotion in hydrogen production in water electrolysis using cellulose nanofluids. However, as an organic nanofluid, the enhancement was caused by the nanostructure of cellulose instead of its thermoelectric properties. Hence, a deeper understanding of the properties of ENF and its performance in hydrogen production through water electrolysis is essential.

In this study, we focused on factors that can affect hydrogen production through water electrolysis. Based on our previous work (Wei et al., 2022), SH electrolyte-based carbon black (CB)-based sodium sulfate electrolyte nanofluids (SSENF) were synthesized. Their stability was compared with aqueous CB nanofluids and CB-based sodium hydroxide electrolyte nanofluids (SHENF). The alkaline ENF was then electrolyzed in a Hoffman apparatus at different nanofluids concentrations. The hydrogen production and current changes with CB concentrations were recorded. In the end, these results were used to build a simplified theoretical model to evaluate the total hydrogen production for alkaline electrolyte-based CB nanofluids. Thus, we investigated the use of electrolyte nanofluids as a substitute for conventional electrolytes in water electrolysis. This approach offers a favorable environment for electrolysis without additional energy consumption. Moreover, it explores the possibility of combining alkaline water electrolysis with photocatalytic water splitting to achieve hydrogen production. To our knowledge, this research is the first to investigate hydrogen production by electrolyzing alkaline ENF. The results are valuable in exploiting the use of nanofluids in hydrogen production.

2. Methodology

2.1. Preparation of nanofluids-based electrolyte

In the first stage of the work, we synthesized nanofluids that were later used for the production of electrolyte nanofluids. The process is shown in Fig. 1. For this, the suitable volume fraction CB particles and 0.5 wt% sodium dodecyl sulfate (SDS) were blended with distilled water and stirred in the mixture until no visible large particle cluster acquired a homogeneous suspension. Then, an ultrasonic bath (Branson 3510E-DTH, 355 W/220–230 V) was used to agitate nanoparticles to make a stable nanofluid. The sample was sonicated for 60 min.

The reason we choose CB nanoparticles as the main object in making nanofluids is that carbon is essentially inert under normal conditions, and it can maintain its properties in a chemical solution and during electrolysis. Therefore, we could focus on the thermal and electrical performance of the nanoparticles in this work. Table 1 shows the physical properties of the CB used in this study.

SDS is an ionic surfactant that is able to stabilize nanofluids (Ulset et al., 2018). It makes nanoparticles possess surface charge, which overlaps with nanoparticles' EDL and makes them repel each other. This stabilization technique is known as electrostatic stabilization. However, SDS shows inadequate performance in breaking large agglomerates and needs sufficient time to respond (Taylor et al., 2013). Hence, we adopt ultrasonic agitation after adding SDS. This technique, known as mechanical stabilization, uses ultrasonic waves on the nanofluid to break down the clusters and agglomerations incidentally (Chung et al., 2009).

Finally, when the stable nanofluid was made, SH bulks were added to the nanofluid and kept stirring until the bulks were wholly dissolved. The magnetic stirring method (Timofeeva et al., 2011), which consists of a ceramic magnet stirrer plate (VWR VMS-C4 advanced, 270 W/230 V) and magnet stirrer bar, was applied for dissolution to maintain the stability of the prepared nanofluid. This process was carried out at room temperature and the stirring speed was set as 1000 rpm.

We chose salt electrolyte in the past (Wei et al., 2022) because it is unable to oxidate nanoparticles. Nonetheless, as a mature technique, the alkaline electrolyzer is widely used in large-scale hydrogen production industries. The purity of produced hydrogen in an alkaline electrolyzer is expected to be more than 99.99%, and the rest of 0.01% is caused by the gas crossover (Ezzahra-Chakik et al., 2017). Schalenbach et al. (2016) experimentally investigated the performance of water electrolysis cells with acidic and alkaline electrolytes. The results showed that alkaline water electrolyzers were more efficient than acidic water electrolysis. The abovementioned advantages make the investigation of nanoparticles in alkaline electrolytes meaningful.

2.2. Experimental procedure

Fig. 2 (a) shows the framework of the experimental setup for the

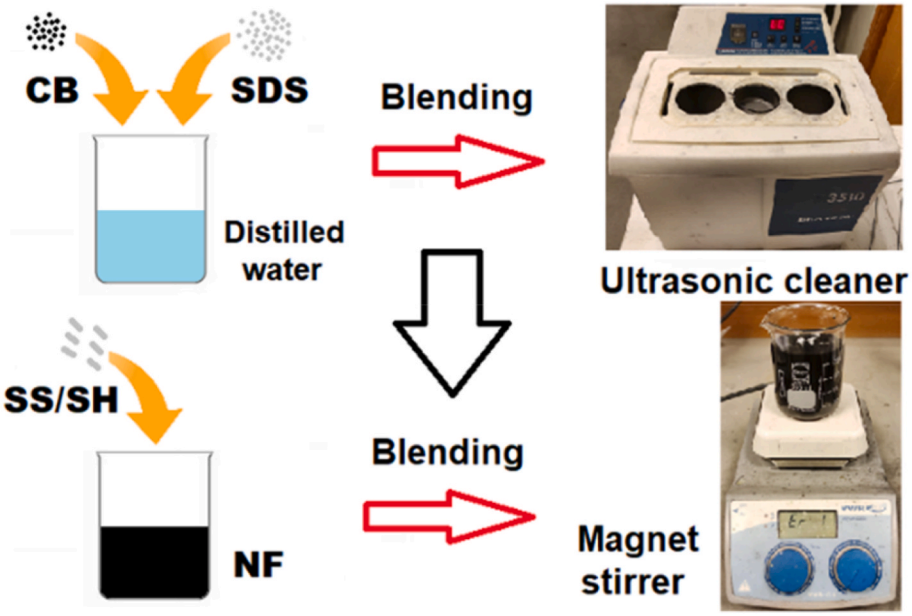

Fig. 1. The process of electrolyte nanofluids' preparation.

Table 1
Properties of carbon black.

Manufacturer	Bulk density	Specific heat	Average particle size	Thermal conductivity
TIMCAL ENSACO™	2250 kg/m^3	710 J/(kg·K)	60 nm	24 W/(m·K)

hydrogen production study. A Hoffman voltameter was used to electrolyze the ENF. CB nanoparticles were unable to be oxidized under the condition of this experiment. Hence, the reactions for alkaline ENF in this work were as follows:

$$\text{Anode: } 2OH^- = H_2O + \tfrac{1}{2}O_2 + 2e^- \quad (1)$$

$$\text{Cathode: } 2H_2O + 2e^- = H_2 + 2OH^- \quad (2)$$

$$\text{Overall Reaction: } H_2O = H_2 + \tfrac{1}{2}O_2 \quad (3)$$

The produced hydrogen and oxygen were gathered at the top of the two vertical pipes of the Hoffman voltameter. The volume of the gases could be read directly from the scale on the pipes with each graduated 60 × 0.2 ml, and the distance between them were 0.1 m. A DC source from Peakteck supplied the power for electrolysis. The maximum output current and voltage were 2 A and 30 V, respectively, and the accuracy

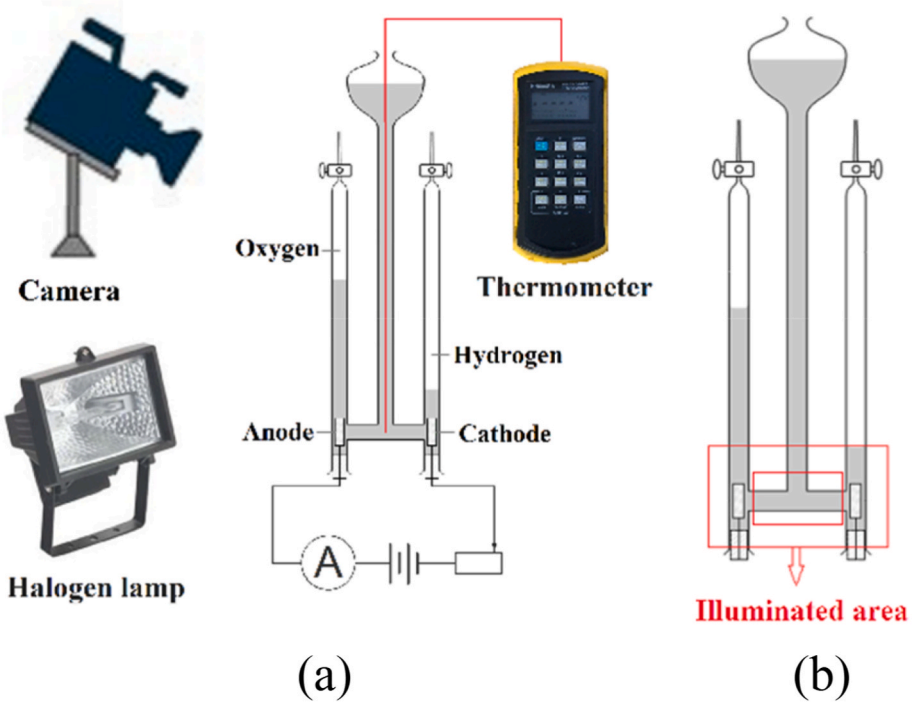

Fig. 2. Schematic representation of experimental apparatus.

was ±1% + 5 digits. A thermocouple was used to test the temperature of the horizontal pipe of the Hoffman voltameter, as shown by the red line in Fig. 2 (a). The temperature could be read and recorded by a data-logger (Omega HH506RA), and its error range was ±0.05%. A halogen lamp (Osram R7S 400 W/230 V) was used to simulate the sun and produce solar radiation. The irradiance was measured by an irradiance meter (Linshang Technology) with an accuracy of ±0.1%. The height of the halogen lamp was set to keep the light bulb and the horizontal pipe on the same level. We adjusted the distance between them to control the irradiance. The irradiance was selected as 1000 W/m^2.

After the ENF was prepared as described in Section 2.1, we filled the Hoffman voltameter until the liquid level reached the tick mark of 0 and closed the outlet of the pipe. The temperature of the prepared ENF was higher than room temperature due to sonification and stirring. Therefore, we let the system in a static condition until the thermal equilibrium was obtained. When the temperature of the sample reached the preset initial temperature (±1 °C.), we turned on the camera, halogen lamp, and DC source simultaneously. In each case, the electrolysis was carried out for 16 min under 30 V voltage input, and the hydrogen production, temperature, and current were recorded every 2 min.

In this study, we focus on the three issues that can affect hydrogen production. The first one is the stability of ENF. Instability has adverse effects on nanofluids' thermophysical and thermoelectrical properties (Sharaf et al., 2020). Thus, the stability of nanofluid-based electrolytes becomes an essential factor affecting hydrogen production and deserves to be investigated. Three different nanofluids with three different concentrations were made in this work. The composition and concentration of each component are shown in Table 2. The nine suspensions were sealed in plastic beakers, as shown in Fig. 3, and recorded their states with photographic equipment every 24 h.

Secondly, the electrolysis experiments were conducted at different initial temperatures. The 0.1 wt% CB ENF with sodium hydroxide concentrations of 1 wt%, 5 wt%, and 10 wt% was electrolyzed. The 10 wt% sodium hydroxide electrolytes without CB were also tested for comparison.

Finally, we performed the electrolysis experiments under different CB concentrations (0.01 wt% ~ 0.3 wt%).

Based on our prior investigation of CB nanofluids, we observed that they exhibit optimal thermal performance within the range of 0.01–0.3 wt% concentration. At lower concentrations, the enhancement provided by the nanoparticles was not evident. Conversely, at higher concentrations, the stability of the nanofluids was affected. Similarly, based on our previous experiments on alkaline electrolyte electrolysis, we found that sodium hydroxide concentrations ranging from 1 to 10 wt% exhibit favorable electrolysis performance and allow for easy observation of the process. At lower concentrations, the electrolysis rate is sluggish, making it challenging to observe changes in the liquid level. Conversely, at higher concentrations, the electrolysis rate becomes excessively rapid, leading to premature consumption of the electrolyte before the preset time.

In this work, two different illuminated areas were set by using a screen to allow the lamp to only irradiate selected regions of the apparatus. The two red rectangles in Fig. 2 (b) show the location and size of the illuminated areas. When the larger illuminated areas, where the area of the main radiation area was approximately 0.015 m^2, were applied, we focused on the thermal properties of ENF. Almost all nanofluids can absorb light energy and make the temperature of the entire system increase fast. Hence, the electrical properties became the main object when using a narrower illuminated area with an area of 0.005 m^2. In this situation, only the nanoparticles dispersed in the path between the two electrodes were irradiated directly. They could affect the motion of ions and currents. In addition, the smaller illuminated area could also diminish the effect of the heat absorption by the metal parts in the system. When a larger irradiation area was employed, both electrodes were also exposed to light, potentially influencing the observed heat and affecting the results. To mitigate this issue, we attempted to cover the electrodes on the pipe using tape. However, the results showed minimal changes, indicating that the effects were limited.

2.3. Evaluation of hydrogen production

The amount of hydrogen produced by electrolysis of alkaline ENF is challenging to calculate, because one needs to consider many factors such as temperature, pressure, concentrations of components, agglomeration of nanoparticles, etc. Therefore, in this study, we focused on the electrical conductivity of nanofluids and explored a simplified correlation with some assumptions on the basis of widely used electrical theories.

The theoretical total hydrogen production can be evaluated by Faraday's law of electrolysis (Godula-Jopek, 2015):

$$n = \frac{It}{zF}, \tag{4}$$

where n is moles of the produced substance at an electrode, respectively, I is current, t is time, z is the valence of the counter-ion, F is the Faraday constant.

The current I can be determined by Ohm's Law for Electromagnetics (Nie et al., 2008):

$$I = \sigma E A, \tag{5}$$

where σ is the electrical conductivity of the electrolyte, in this study, it is the electrical conductivity of the alkaline ENF, E is the electric field, and A is the area that the charge flows through.

While the thermal conductivity of nanofluids has been extensively studied, the investigation of their electrical conductivity remains incomplete. Currently, there are three theoretical models used for electrical conductivity analysis: the Maxwell model (Maxwell, 1873), the Bruggeman model (Bruggeman, 1935), and the Fricke model (Fricke, 1924). Among these models, the Maxwell model demonstrates higher precision than the Bruggeman model at low concentrations for spherical particles. On the other hand, the Fricke model accounts for general particles, but its accuracy is inferior to that of the Maxwell model when applied specifically to spherical particles (Minea, 2019). Therefore, the electrical conductivity of the ENF is determined by the electrical conductivity of the base fluid (SH solution) and the electrical conductivity of CB nanoparticles, and it can be calculated by the Maxwell model (Maxwell, 1873):

$$\sigma = \sigma_f \left[1 + \frac{3\left(\frac{\sigma_p}{\sigma_f} - 1\right)\varphi}{\frac{\sigma_p}{\sigma_f} + 2 - \left(\frac{\sigma_p}{\sigma_f} - 1\right)\varphi} \right], \tag{6}$$

where σ is the electrical conductivity of the ENF; σ_f is the electrical

Table 2
Composition and concentration of samples.

Samples	1	2	3	4	5	6	7	8	9
Composition and concentration (wt.%)	CB/0.05 SDS/0.5 – Distilled water	CB/0.1	CB/0.5	CB/0.05 SH/5	CB/0.1	CB/0.5	CB/0.05 SS/10	CB/0.1	CB/0.5

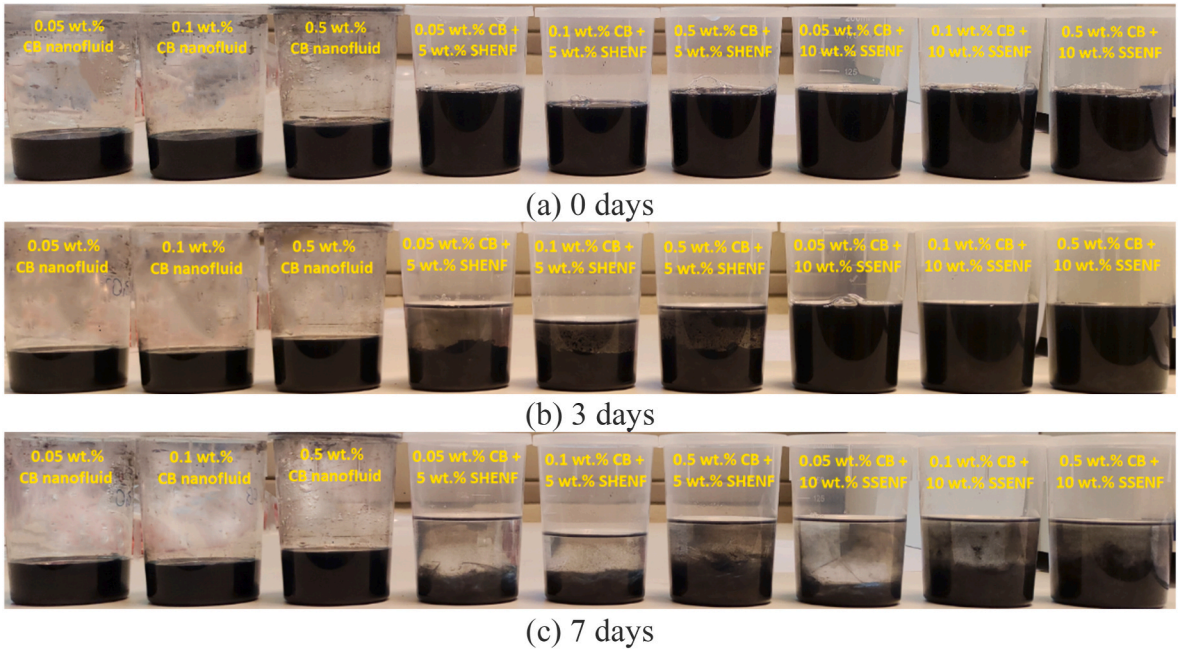

Fig. 3. Photographs of the different suspensions (CB nanofluids, CB/SHENF, CB/SSENF) at different times.

conductivity of the base fluid; σ_p is the electrical conductivity of the particles, and φ is the concentration of the nanofluid. Normally, the concentration of nanofluids is less than 1 wt%, which means that term $(\frac{\sigma_p}{\sigma_f}+2)$ is at least two orders of magnitude less than the term $\left(\frac{\sigma_p}{\sigma_f}-1\right)\varphi$ is at least 2 orders of magnitude smaller. Therefore this small term can be ignored in equation (6).

However, many researchers reported that the Maxwell model has low accuracy as it only considers the electrical properties of nanoparticles and neglects the motion of nanoparticles in nanofluids (Said et al., 2022). Hence, Shen et al. (2012) proposed a new model that takes electrophoresis and Brownian motion into consideration on the basis of the Maxwell model. In his model, the electrical conductivity enhanced by electrophoresis can be given by:

$$\sigma_E = \frac{2\varphi\varepsilon_d{}^2\varepsilon_{d0}{}^2\zeta^2}{\mu r^2}, \tag{7}$$

where σ_E is the electrical conductivity due to electrophoretic mobility; ε_d is the dielectric constant of base fluid; ε_{d0} is the dielectric constant of vacuum; ζ is the zeta potential of nanoparticles that will be discussed in detail in Section 3.1; μ is the viscosity of the nanofluid and r is the radius of nanoparticles.

Also, the electrical conductivity enhanced by Brownian motion is (Shen et al., 2012):

$$\sigma_B = \frac{3\varphi\varepsilon_d\varepsilon_{d0}\zeta\left(\frac{RT}{L},\frac{1}{3\pi\mu}\right)}{r^{\frac{3}{2}}}, \tag{8}$$

where σ_B is the electrical conductivity caused by Brownian motion, R is the thermodynamic constant, T is temperature, and L is the Avogadro constant.

Therefore, by combining equation (6) ~ (8) and implementing them into equation (5), the current I can be written as:

$$I = \left\{\sigma_f\left[1+\frac{3\left(\frac{\sigma_p}{\sigma_f}-1\right)\varphi}{\frac{\sigma_p}{\sigma_f}+2-\left(\frac{\sigma_p}{\sigma_f}-1\right)\varphi}\right]+\frac{2\varphi\varepsilon_d{}^2\varepsilon_{d0}{}^2\zeta^2}{\mu r^2}+\frac{3\varphi\varepsilon_d\varepsilon_{d0}\zeta\left(\frac{RT}{L},\frac{1}{3\pi\mu}\right)}{r^{\frac{3}{2}}}\right\}EA, \tag{9}$$

To simplify equation (9), some assumptions were adopted. First, the stability of the nanofluids must be assured, which means that no aggregation and deposition are formed during the electrolysis. Hence, the radius of nanoparticles and zeta potential can be treated as constant. Second, the change of electrical conductivity due to concentration change during the electrolysis can be ignored as the process duration was rather short. Third, we evaluated the Brownian motion conductivity and electrophoretic conductivity, and found that the temperature change had less impact on the Brownian motion conductivity, as well as the overall electrical conductivity. Thus, the temperature effects on total electrical conductivity are negligible. Therefore, equation (9) can be simplified as follows:

$$I = \sigma_f EA + \left[\frac{3\left(\frac{\sigma_p}{\sigma_f}-1\right)\sigma_f}{\frac{\sigma_p}{\sigma_f}+2}+\frac{2\varepsilon_d{}^2\varepsilon_{d0}{}^2\zeta^2}{\mu r^2}+\frac{3\varepsilon_d\varepsilon_{d0}\zeta\left(\frac{RT}{L},\frac{1}{3\pi\mu}\right)}{r^{\frac{3}{2}}}\right]EA\varphi = \mathscr{A}+\mathscr{B}\varphi. \tag{10}$$

From the discussion above, $\mathscr{A}$ and $\mathscr{B}$ can be considered constant. These can be treated as fitting empirical parameters.

3. Results and discussion

3.1. Stability of the nanofluids-based electrolyte

In this study, an observation of the time-dependent sedimentation method was used to test the stability of ENF, which is considered an effective way to confirm nanofluids' stability (Li et al., 2020). In Table 1, samples 1–3 and 7–9 are set for comparison. The results are shown in Fig. 3. These photos were taken after the suspensions were prepared, after three days, and after seven days.

The aqueous CB nanofluids (see the first three images in Fig. 3(c)) showed excellent stability as expected (Ulset et al., 2018). However, both the sodium sulfate electrolyte nanofluids (SSENF) and the sodium hydroxide electrolyte nanofluids (SHENF) maintained their stability for a short time and then deteriorated, where the stability of SHENF were worse than SSENF. According to our observation, the distinguishable small clusters were formed after two days, three days, and three days in the SHENF at the CB concentration of 0.5 wt%, 0.1 wt%, 0.05 wt%,

respectively. The visible sedimentation that can be identified in the graphics appeared after seven days. However, there was no visible sedimentation in SSENF after three days, as seen in Fig. 3(b) A possible explanation is that the particles had already agglomerated, but their sizes were still very small and the dark environment made them difficult to observe.

The existence of SH significantly increases the pH of nanofluids. Also, pH can be slightly increased by adding SS. With the increase in pH, the zeta potential decreases due to electrochemical charge neutralization on the surface of CB nanoparticles, which deteriorates the EDL (Kessler et al., 2019). When the pH reaches the isoelectric point, the zeta potential becomes zero. Some researchers found the isoelectric point of graphene to correspond to a pH of 7.5 (Zuccaro et al., 2015). It should be noted that the isoelectric point is very sensitive to the particle size, and smaller particles have higher isoelectric points (Alnarabiji and Husein, 2020). Therefore, it is reasonable to assume the isoelectric point of CB nanofluids is higher than 7.5, which makes SHENF show worse stability than SSENF.

Zeta potential is an important parameter indicating the stability of nanofluids. Ohshima (2003) suggested that when the surface charge is very high, zeta potential is equal to the critical zeta potential, where the repulsive force is equal to the maximum van Der Waals force according to Derjaguin-Landau-Verwey-Overbeek (DLVO) theory. The critical zeta potential can be calculated by (Teh et al., 2010):

$$\zeta = \frac{k_B T}{ze} ln \frac{1}{\varphi}, \tag{11}$$

where, k_B is the Boltzmann constant, e is the elementary electric charge, φ is the volume fraction of primary particles given by (Prasher et al., 2006):

$$\varphi = \varphi_p \varphi_a, \tag{12}$$

where φ_p is the volume fraction of the particles in the aggregates, φ_a is the volume fraction of the aggregates in the nanofluid.

The process of sedimentation in SHENF could be divided into three stages. When SHENF were prepared, almost no aggregate in the fluid exists. Hence, $\varphi_p = 1$, and $\varphi = \varphi_a$, where the nanoparticles were also treated as aggregates in the model. First, the nanoparticles formed aggregates and grew, but they were hard to observe. In our tests, this stage occurred in the first two days. In the second stage, when the aggregates grew large enough, the deposition appeared due to gravity. During this time, φ increased as the volume of aggregates increased, leading to a decrease in critical zeta potential, as shown by equation (11). In the meantime, small agglomerations still existed and dispersed in the liquid. The sedimentation was mixed as shown in Fig. 3 (b). In our experiments, this stage lasted for about three days until the fully sedimented stage, where $\varphi_a = 1$, and $\varphi = \varphi_p$. In this final stage, almost all the particles were sedimented in the base fluid. However, flocculate suspensions were observed above the surface of sedimentation, as shown in Fig. 3.

Ali et al. (2019) divided the sedimentation behaviour of nanofluids into three categories, namely, dispersed sedimentation, flocculated sedimentation, and mixed sedimentation. They concluded that the flocculated sedimentation in aluminum nanofluids was caused by the nanoparticle's oxidation. According to Leong and Ong (2003), when the zeta potential of a stable colloidal dispersion reached the critical zeta potential, it started to transmit to a flocculated dispersion, in which the viscosity of flocculated dispersion was several orders of magnitude larger than its stable state.

Commonly, in a stationary container without any external force except gravity, the aggregation of nanoparticles is caused by Brownian motion regardless of the thermal boundary resistance between the particles and the base fluid (Prasher et al., 2006). The aggregation in a nanofluid with time can be described as (Hanus et al., 2001):

$$\frac{R_a}{r} = \left(1 + \frac{t}{t_a}\right)^{\frac{1}{d_f}}, \tag{13}$$

where R_a is the gyration radius of the aggregates, t is the time, t_a is the aggregation time constant, d_f is the fractal dimension of the aggregates. Waite et al. (2001) suggested that d_f was in the range of 1.8–2.3. For the Brownian agglomeration, the fractal dimensions is lower than 2

The aggregation time constant t_a is given by:

$$t_a = \frac{\pi \mu r^3 W}{k_B T}, \tag{14}$$

where W is the stability ratio. When $W = 1$, there is no repulsive force as well as hydrodynamic interactions between the nanoparticles in the presence of a repulsive force, $W > 1$. According to DLVO theory, stability ratio W can be calculated by the repulsive and attractive potential energies. It is a strong function of nanoparticles radius r, as W decreases rapidly with decreasing r (Prasher et al., 2006).

Following equation (14), the aggregation time constant t_a decreases with the decrease in particle size, which indicates smaller particles are more prone to agglomerate. When SS or SH is added to CB nanofluids, the repulsive force potentially deteriorates, which induced a decrease in W. Furthermore, equation (13) indicates the growth speed of aggregates will become slower with time, which shows an agreement with our results, as seen in Fig. 3.

Therefore, the stability states of SHENF make them become made-and-use instantly samples. Many researchers also confirmed this conclusion (Liu et al., 2016; Wang and Wang, 2016), and there is no suitable method to maintain the stability of ENF as it is possible for standard nanofluids at present.

3.2. Effect of nanoparticles on total hydrogen production

In this study, the hydrogen production from the electrolysis of a 10 wt% SHENF with 0.1 wt% CB was presented, and the results were compared with the hydrogen production from the electrolysis of a 10 wt % SH solution. The light and SDS were applied in both systems. Fig. 4 shows the comparison results. The hydrogen was produced in a greater amount and also faster in SHENF than in SH solution. For SHENF, it took 7 min to reach the maximum hydrogen volume of 57.9 ml. However, the maximum hydrogen volume of 60.2 ml was achieved at 9 min for SH solution. This indicates the hydrogen production rate for SHENF was about 23.61% higher than the SH solution.

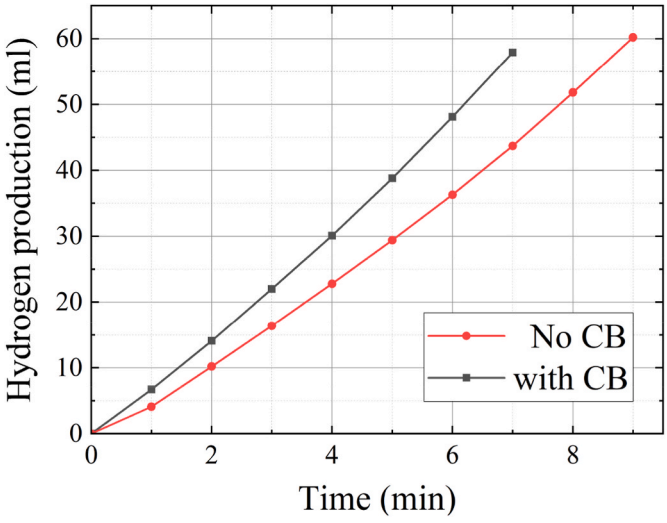

Fig. 4. Hydrogen production for 10 wt% SH electrolytes at different time with and without CB (φ = 0.1 wt%, $T_{initial}$ = 30 °C).

Obliviously, CB particles played an essential role in the process. As discussed in Section 2.3, the enhancement of electrical conductivity caused by electrophoresis and Brownian motion has a positive impact on hydrogen production.

Another reason is the enhancement of mass transfer induced by nanoparticles. In the electrical field, the motion of nanoparticles is empowered by Brownian motion and electrophoresis as well. The velocity of Brownian motion for a single particle or cluster can be calculated from (Beiki et al., 2013a,b):

$$v_B = \sqrt{\frac{9k_BT}{4\rho\pi r^3}}, \tag{15}$$

where v_B is the velocity of Brownian motion, ρ is the density of nanoparticles.

The velocity of a particle caused by electrophoresis can be calculated by the electrophoretic mobility formula (Huckel, 1924):

$$\mu_E = \frac{v_P}{E} = \frac{2\varepsilon_p\varepsilon_{p0}}{3\mu}\zeta, \tag{16}$$

where μ_E is the electrophoretic mobility, v_P is the velocity of electrophoresis, ε_p is the relative permittivity of the fluid, ε_{p0} is the permittivity of a vacuum.

The viscosity μ is a temperature-sensitive parameter, decreasing with the temperature increase. Following equations (15) and (16), v_B and v_P increase with temperature, which induces higher convective mass transfer at higher temperatures. Fig. 5 shows the temperature history with and without CB. The presence of the CB improved the temperature-increasing pattern due to the enhanced thermal conductivity of the fluid. Therefore, the mass transfer was stronger in SHENF. This conclusion can be confirmed by Beiki et al. (2013a,b). They investigated the convective mass transfer of Al_2O_3 and TiO_2 ENF in a circular tube and discovered a higher mass transfer ratio in laminar flow. According to Fig. 5, when CB was introduced into the electrolyte, the temperature exhibited a rapid increase and reached 45 °C within 6 min, compared to 40 °C without CB. This higher temperature corresponded to a 23.61% increase in production, requiring no additional energy consumption apart from the application of CB. Therefore, the utilization of nanoparticles in the electrolyte demonstrates the potential to reduce energy consumption.

Furthermore, the two explanations mentioned above are the primary reason that CB nanofluids improved hydrogen production. However, there are still some factors that can potentially affect hydrogen production. Although they have limited influence, they are still worth discussing.

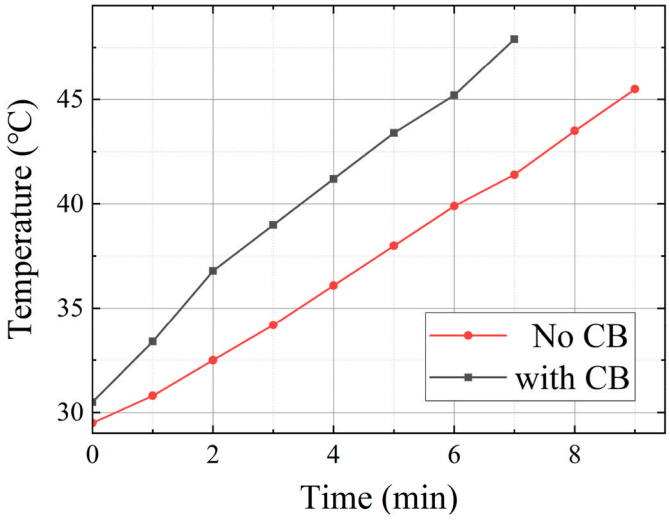

Fig. 5. Temperature increases for 10 wt% SH electrolytes at different time with and without CB (φ = 0.1 wt%, $T_{initial}$ = 30 °C).

The first factor is that nanoparticles adhered to the electrodes. This fact was also noticed by Choi and Lee (2020), who reported the cellulose nanofluid was coated on the anode. They state this phenomenon indeed hindered the process of electrolysis and reduced gas production. Nevertheless, in our work, the CB nanoparticles did not fully cover the electrodes: we estimate that more than 50% of the electrode area was clean from the nanoparticles. Indeed, this partial deposition by carbon nanoparticles may be beneficial for the process: the presence of the particles may enhance the electrical conductivity and expand the surface area. According to Ghosh and Subudhi (2022), carbon nanotubes have been widely used as electrodes in microbial fuel cells and proton exchange membrane fuel cells as their high aspect ratio, low weight, and high conductivity. Therefore, it is reasonable to assume the CB nanoparticle coating on electrodes has a positive impact on electrolysis.

The second factor is the formation of bubbles. SDS was used to stabilize the ENF, however, it caused the formation of bubbles during the electrolysis. On the other hand, to diminish other chemicals to affect the properties of ENF, we did not add anti-foam in the preparation of ENF. According to Wang et al. (2014), the effect of bubbles can be divided into two types, namely bubble coverage on electrodes and bubble dispersion in an electrolyte. In our experiments, as mentioned in the previous paragraph, the presence of CB in the electrolyte resulted in the adhesion of nanoparticles, which coated the electrodes and prevented bubbles from adhering to them. Hence, the suspension of bubbles became the main behavior of the bubble effect. Correspondingly, this behavior was not obvious in the samples without CB. Bubbles can increase the void fraction which leads to large electrolyte resistance, and extra energy consumption (Matsushima et al., 2012).

The third factor is the potential caused by the sedimentation of aggregates. This interesting assumption was proposed by Ohshima (2003), who investigated the velocity of sedimentation and the potential of sedimentation using the Stokes formula. The findings revealed that the sedimentation potential is highly dependent on the radius of the aggregate. Nevertheless, this factor has limited effects on a stable ENP.

3.3. Effect of initial temperature

As an essential factor in electrolysis, the temperature can affect the activity of substances and reaction rate. In this work, we tested the total hydrogen production at different initial temperatures with different SH concentrations, as shown in Fig. 6. The concentration of CB nanofluids was 0.1 wt%. As expected, the total hydrogen production increases with the growth of initial temperature and SH concentration.

This result is consistent with the findings of Hiraki et al. (2005), who investigated the reaction rates when the range of the initial temperature was 291 K–333K. Their study revealed that the initial temperature of NaOH solutions had a significant impact on the reaction rate. Specifically, when the initial temperature was set to 313 K or above, the reaction was completed within 1200 s in their experimental set-up. However, when the temperature was set to 291 K, the generation of hydrogen continued for more than 2400 s.

The reaction rate constant depends on several factors, including temperature, pressure, etc. The relationship between the reaction rate constant and temperature can be described by the Arrhenius equation (Crapse et al., 2021):

$$k_a = A_a e^{-\frac{E_a}{RT}} \tag{17}$$

where k_a is the reaction rate constant, A_a is an exponential factor that is a constant for a given chemical reaction, relating the frequency of collisions of atoms and molecules, E_a is the activation energy of the reaction.

Based on Equation (17), a higher initial temperature results in a faster reaction rate, which in turn leads to an increase in the amount of hydrogen produced. Additionally, during the electrolysis process, the

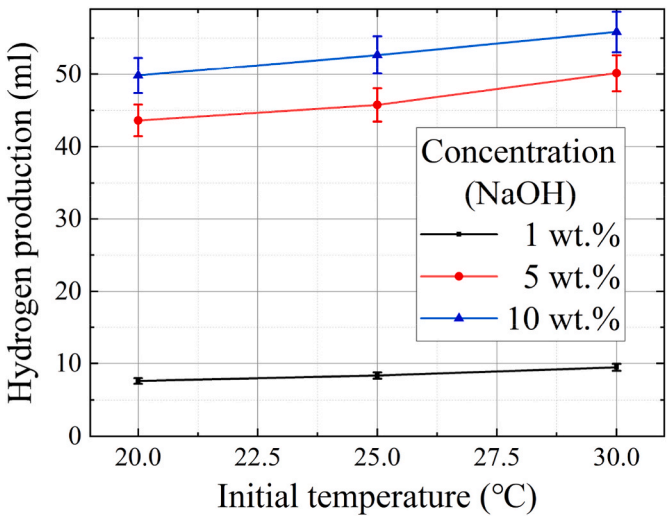

Fig. 6. Total hydrogen production at different initial concentrations (φ = 0.1 wt%).

nanoparticles absorb radiation, which causes the temperature of the electrolyte to rise even further, thus accelerating the reaction rate even more.

3.4. Effect of CB concentration

Fig. 7 depicts the comparison of hydrogen production at different CB concentrations for two cases: (i) with the screen; (ii) without the screen. These experiments were conducted at the initial temperature of 30 °C, and the concentration of sodium hydroxide was 5 wt%. In both studied cases, the total hydrogen production shows the tendency to increase first and then decrease with the growth of the CB concentration. For no screen case, the maximum production occurred at 0.04 wt%, while when the screen was used the maximum hydrogen production showed at a higher concentration.

The increasing tendency was caused by the following reasons. Firstly, equations (6) and (7) indicated that an increase in CB concentration φ led to an increase in electrical conductivity caused by electrophoresis σ_E and Brownian motion σ_B, respectively. Secondly, according to equation (11), zeta potential ζ was proportional to the temperature T. Hence, it could be seen from equations (15) and (16) that the particle velocity of electrophoresis v_E and Brownian motion v_B increased with the rising of temperature, which improved the mass transfer in the ENF. Thirdly, the convective heat transfer was enhanced by the applied electrical field (Sheikholeslami and Bhatti, 2017), leading to faster temperature. Additionally, CB nanoparticles might have formed a chain-shaped conducive path in the fluid, which escalated the electrical conductivity. Lastly, the strengthening of EDL was also a possible reason that was discussed in our previous study (Wei et al., 2022).

The reason for the decreasing tendency was mainly caused by the agglomerations and sedimentation of CB nanoparticles. The agglomeration meant the growth of particle size r. Hence, the electrical conductivity and mass transfer enhanced by electrophoresis and Brownian motion were diminished, according to equations ((6), (7), (11), (15) and (16). In addition, the total mass transfer in the ENF is affected by the Brownian Reynolds number, which is given by (Prasher et al., 2006):

$$Re = \frac{2v_B r\rho}{\mu}, \tag{18}$$

And the thermal conductivity of ENF is given by (Prasher, 2005):

$$\frac{k}{k_0} = 1 + A \times Re^m \, Pr^{0.333} \, \varphi, \tag{19}$$

where k is the thermal conductivity, k_0 is the thermal conductivity of the base fluid, A and m are constants measured by experiments, Pr is the Prandtl number.

Prasher et al. (2006) reported that aggregation can significantly decrease the Brownian Reynolds number, which also worsens the thermal conductivity, as seen in equation (19). Also, according to Beiki et al. (2013a,b), the mass transfer coefficient for Al_2O_3 ENF increased with the concentration of nanofluids up to 0.01% and then decreased, which corresponds to our conclusions.

Secondly, the chain-shaped conductive path did not always assist the electrical conductivity. When the aggregates became large enough, the path formed a considerable resistance, which could hinder the current and reaction and reduce hydrogen production.

Lastly, the high concentration of CB was able to form a "shield", which could block the mass transfer and the penetration of light. Then, causing the deteriorated thermal performance of nanofluids.

Furthermore, the use of the screen had little effect on hydrogen production, as seen in Fig. 8. The maximum hydrogen production was 52 ml at 16 min when the screen was applied, corresponding to the 57 ml of the case without the screen. Thus, the production was 9% lower. However, the difference in the temperature was significant, as shown in

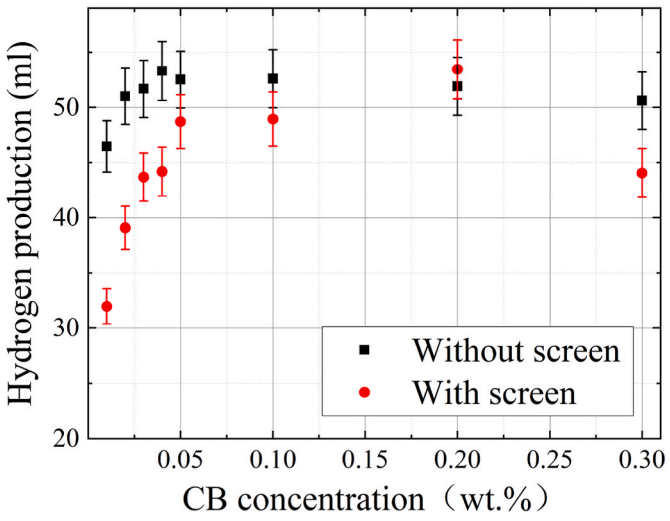

Fig. 7. Total hydrogen production vs. different CB concentrations with and without the screen ($\varphi_{(NaOH)}$ = 5 wt%, $T_{initial}$ = 30 °C).

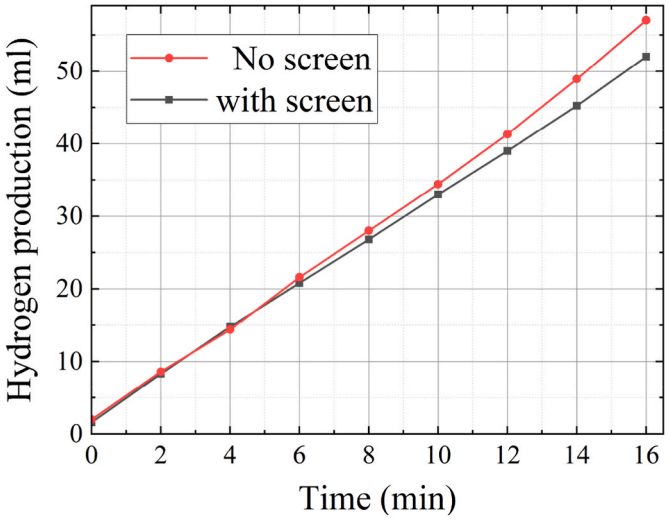

Fig. 8. Hydrogen production for 0.05 wt% CB SHENF at different times with and without the screen ($\varphi_{(NaOH)}$ = 5 wt%, $T_{initial}$ = 30 °C).

Fig. 9. The larger illuminated area allowed more heat to be absorbed, and the temperature increased faster. Whereas a higher temperature can make the formation of aggregation faster, according to equations (13) and (14). Hence, the negative impact of CB nanofluids showed at lower CB concentrations for the case without the screen, as shown in Fig. 7. On the other hand, there was a temperature gradient between the illuminated area and the unilluminated area. Temperature gradient facilitated the convective heat transfer, as well as mass transfer. Improved mass transfer, coupled with enhanced electron movement, can increase the rate of electrolysis, resulting in greater hydrogen production. This phenomenon also resulted in enhanced electron movement, indicative of the electrolysis rate. These convective transfers were more significant when the screen was used, leading to an increased hydrogen production.

Moreover, the better performance for the smaller illuminated case showed that the electrical properties played a more important role than thermal properties. This phenomenon indicates that the enhancement of light mainly occurred in the current path area. A concentrated light can be used in further investigation to save energy.

3.5. Relationship between the current and CB concentrations

According to the conclusions of the previous section, we decided to use the current data recorded in the electrolysis of SHENF with the screen, as they showed better stability and were potentially used in industries.

As discussed in Section 2.3, a critical parameter to evaluate the total hydrogen production for electrolysis in SHENF is current, as seen in equation (4). The black dots in Fig. 10 show the average current at different CB concentrations. The average current history exhibits a similar tendency as hydrogen production. It increased first and then decreased, with the maximum current shown at the CB concentration of 0.1 wt%. In the previous section, we analyzed that the high concentrations of CB had a negative impact on the electrical conductivity of ENF. This conclusion can be proved by Fig. 10. However, when the CB concentration was higher than 0.1 wt%, the adverse effects on the electrical conductivity caused the current to decrease. In the meantime, nanofluids' thermal properties still played an important role in promoting hydrogen production, which made the highest hydrogen production shown at the concentration of 0.2 wt%.

According to equation (10), the current has a linear relationship with CB concentration. However, some assumptions are not met at higher CB concentrations, such as the assumption of no agglomeration in the SHENF during the electrolysis process. Hence, we focused on the lower

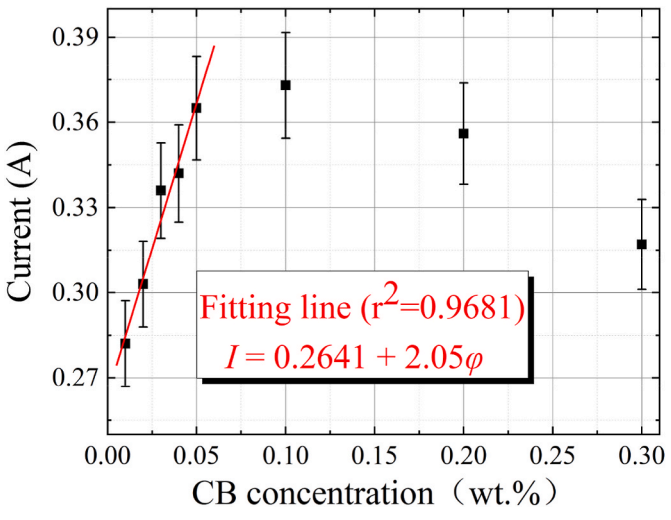

Fig. 10. Current vs. CB concentration and fitting line ($\varphi_{(NaOH)}$ = 5 wt%, $T_{initial}$ = 30 °C, screen applied).

CB contractions, namely $\varphi < 0.05$ wt.%., which showed better stability and allow us to evaluate the hydrogen production

The fitting result is shown in the red line of Fig. 10. Generally, the efficiency of hydrogen production is less than 100%. Hence, we introduced a correction factor η that indicates the different processes of electrolysis. According to our calculation, when a screen is applied in the electrolysis, η becomes 0.57. Substituting the fitting result and correction factor η into equation (4), it becomes:

$$n(H_2) = 0.57\frac{(0.2641 + 2.05\varphi)t}{2F}, \tag{20}$$

Fig. 11 shows the comparison of hydrogen production between the experimental results and calculation results from equation (20). The calculation results show a good agreement with the experimental results when the CB concentrations are below 0.1 wt%. The errors are shown in Table 3.

Equation (20) is a simplified model with considerable limitations. The most important one is that it does not take agglomeration into consideration. However, the agglomeration process is very random, similar to the Brownian motion. Some researchers have presented models that may forecast agglomeration. Equations (13) and (14) were built based on the effect of aggregate radius on repulsive force and

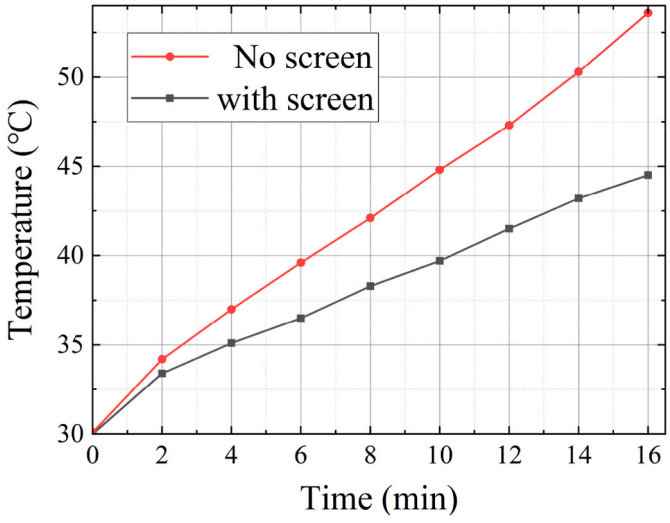

Fig. 9. Temperature for 0.05 wt% CB SHENF at different times with and without the screen ($\varphi_{(NaOH)}$ = 5 wt%, $T_{initial}$ = 30 °C).

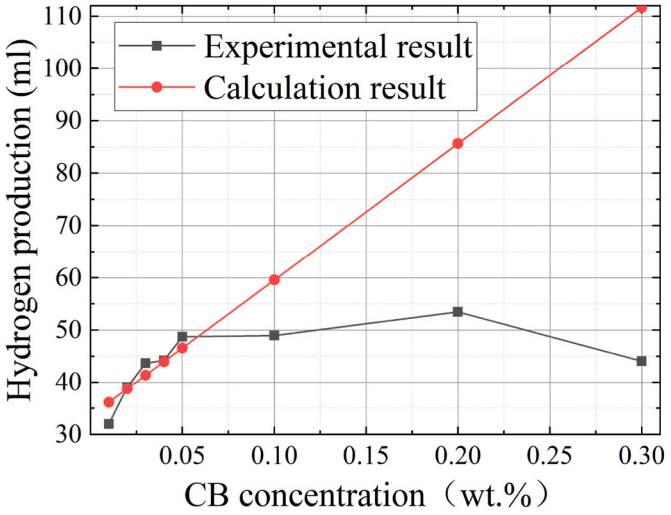

Fig. 11. Comparison between experimental and calculation results ($\varphi_{(NaOH)}$ = 5 wt%, $T_{initial}$ = 30 °C, screen applied).

Table 3
Error analysis of experimental results and simulation results.

CB concentration/wt.%	0.01	0.02	0.03	0.04	0.05	0.10	0.20	0.30
Hydrogen production (experiments)/ml	31.98	39.08	43.69	44.20	48.71	48.95	53.45	44.07
Hydrogen production (simulations)/ml	36.16	38.76	41.36	43.97	46.57	59.59	85.64	111.68
Error	0.115	−0.008	−0.056	−0.005	−0.0459	0.179	0.376	0.605

attractive force (Prasher et al., 2006), but the impacts of the electrical field were not included. Similarly, Ohshima took the density difference between nanoparticles and base fluids into account (Ohshima, 2003), but the effect of the electrical field was absent. Therefore, the direction to optimize equation (20) is to find the agglomeration and sedimentation behavior in an electrical field.

4. Conclusions

In this study, SHENF was prepared, and its stability was investigated. The electrolysis experiments were conducted in a Hoffman voltameter at different initial temperatures, SH concentrations and CB contractions, and the results were used to build a model to evaluate the total hydrogen production. A possible technical method to assess the total hydrogen production was presented, and a simplified model was built to evaluate the total hydrogen production for electrolysis SHENF with a screen. Some of the crucial conclusions are as follows:

- The presence of salt or alkaline solution can weaken the stability of CB nanofluids, and CB nanoparticles were fully sedimented in seven days in SHENF.
- CB nanoparticles can improve the hydrogen production of electrolysis by the enhancement of electrical conductivity, mass transfer, and heat absorption. The hydrogen production rate was improved by 23.62% when 0.1 wt% CB was applied in 10 wt% SHENF.
- The initial temperature had an impact on the hydrogen production
- For electrolysis of SHENF, the total hydrogen production increased with the increases in CB concentration and then decreased. When employing a screen, the maximum hydrogen production showed at the concentration of 0.2 wt%, whereas the maximum hydrogen production showed at the concentration of 0.04 wt% without a screen.

A semi-empirical correlation was proposed to evaluate the total hydrogen production for electrolysis of SHENF with a screen, which had a higher precision when the CB concentrations were below 0.1 wt%

According to our research, it is an interesting problem to use nanofluids for water electrolysis. This may create a new path to connect solar energy and hydrogen, which is meaningful for the energy industry. However, there are limitations to be acknowledged in this study. While alkaline electrolyte is generally favorable for water electrolysis, it is not suitable for nanofluids since their stability is best maintained at a pH value of around 4–5. Consequently, the use of alkaline electrolyte nanofluids is effective only for a limited duration before their stability deteriorates. This can pose challenges for implementing this method on a large scale if stability cannot be maintained. Furthermore, the performance of CB ENF under high pressure and temperature, commonly encountered in industrial water electrolysis, is difficult to predict and requires further investigation. Hence, two important issues should be investigated in further work. The first one is finding a better method to enhance the stability of ENF. Another one is building a model that describes how the electrical field influences the aggregation and sedimentation of nanoparticles.

CRediT authorship contribution statement

Shihao Wei: Conceptualization, Investigation, Writing – original draft. **Boris V. Balakin:** Methodology, Writing – review & editing, Supervision. **Pawel Kosinski:** Conceptualization, Resources, Writing – review & editing, Supervision.

Declaration of competing interest

The authors declare that they have no known competing financial interests or personal relationships that could have appeared to influence the work reported in this paper.

Data availability

Data will be made available on request.

Acknowledgments

Shihao Wei gratefully acknowledges financial support from the China Scholarship Council.

Boris Balakin thanks the Norwegian Research Council for funding (project 300286).

References

Ali, N., Teixeira, J.A., Addali, A., 2019. Aluminium nanofluids stability: a comparison between the conventional two-step fabrication approach and the controlled sonication bath temperature method. J. Nanomater. 1–9, 2019.
Alnarabiji, M.S., Husein, M.M., 2020. Application of bare nanoparticle-based nanofluids in enhanced oil recovery. Fuel 267, 117262.
Bagheli, S., Fadafan, H.K., Orimi, R.L., Ghaemi, M., 2015. Synthesis and experimental investigation of the electrical conductivity of water based magnetite nanofluids. Powder Technol. 274, 426–430.
Beiki, H., Esfahany, M.N., Etesami, N., 2013a. Turbulent mass transfer of Al_2O_3 and TiO_2 electrolyte nanofluids in circular tube. Microfluid. Nanofluidics 15, 501–508.
Beiki, H., Esfahany, M.N., Etesami, N., 2013b. Laminar forced convective mass transfer of γ-Al_2O_3/electrolyte nanofluid in a circular tube. Int. J. Therm. Sci. 64, 251–256.
Bruggeman, V.D., 1935. Berechnung verschiedener physikalischer Konstanten von heterogenen Substanzen. I. Dielektrizitätskonstanten und Leitfähigkeiten der Mischkörper aus isotropen Substanzen. Annalen derhysic 416 (7), 636–664.
Buttler, A., Spliethoff, H., 2018. Current status of water electrolysis for energy storage, grid balancing and sector coupling via power-to-gas and power-to-liquids: a review. Renew. Sustain. Energy Rev. 82, 2440–2454.
Choi, D., Lee, K.Y., 2020. Experimental study on water electrolysis using cellulose nanofluid. Fluid 5 (4), 166.
Chung, S.J., Leonard, J.P., Nettleship, I., Lee, J.K., Soong, Y., Martello, D.V., Chyu, M.K., 2009. Characterization of ZnO nanoparticle suspension in water: effectiveness of ultrasonic dispersion. Powder Technol. 194 (1–2), 75–80.
Crapse, J., Pappireddi, N., Gupta, M., Shvartsman, S.Y., Wieschaus, E., Wühr, M., 2021. Evaluating the Arrhenius equation for developmental processes. Mol. Syst. Biol. 17 (8), e9895. https://doi.org/10.15252/msb.20209895.
David, M., Ocampo-Martínez, C., Sánchez-Peña, R., 2019. Advances in alkaline water electrolyzers: a review. J. Energy Storage 23, 392–403.
El-Emam, R.S., Özcan, H., 2019. Comprehensive review on the techno-economics of sustainable large-scale clean hydrogen production. J. Clean. Prod. 220, 593–609.
Ezzahra Chakik, F., Kaddami, M., Mikou, M., 2017. Effect of operating parameters on hydrogen production by electrolysis of water. Int. J. Hydrogen Energy 42 (40), 25550–25557.
Fricke, H., 1924. A mathematical treatment of the electric conductivity and capacity of disperse systems I. The electric conductivity of a suspension of homogeneous spheroids. Phys. Rev. 24 (5), 575.
Ghosh, S., Subudhi, S., 2022. Developments in fuel cells and electrochemical batteries using nanoparticles and nanofluids. Energy Storage 4 (3), e288.
Godula-Jopek, A., 2015. Hydrogen Production: by Electrolysis. John Wiley & Sons.
Grigoriev, S.A., Fateev, V.N., Bessarabov, D.G., Millet, P., 2020. Current status, research trends, and challenges in water electrolysis science and technology. Int. J. Hydrogen Energy 45 (49), 26036–26058.
Hanus, L.H., Hartzler, R.U., Wagner, N.J., 2001. Electrolyte-induced aggregation of acrylic latex. 1. Dilute particle concentrations. Langmuir 17 (11), 3136–3147.
Hiraki, T., Takeuchi, M., Hisa, M., Akiyama, T., 2005. Hydrogen production from waste aluminum at different temperatures, with LCA. Mater. Trans. 46 (5), 1052–1057.
Huckel, E., 1924. Die kataphorese der kugel. Phys. Z. 25, 204–210.

Kessler, J.C., Padoin, N., Hotza, D., Soares, C., 2019. Rheological behavior of a silver aqueous nanofluid stabilized with aminosilane-based surfactant under confined flow. Braz. J. Chem. Eng. 36, 229–237.
Khan, U., Ahmed, N., Mohyud-Din, S.T., Bin-Mohsin, B., 2016a. A bioconvection model for MHD flow and heat transfer over a porous wedge containing both nanoparticles and gyrotatic microorganisms. J. Biol. Syst. 24 (4), 409–429.
Khan, U., Ahmed, N., Mohyud-Din, S.T., 2016b. Influence of viscous dissipation and Joule heating on MHD bio-convection flow over a porous wedge in the presence of nanoparticles and gyrotactic microorganisms. SpringerPlus 5, 1–18.
Kim, J., Park, H., 2021. Enhanced mass transfer in nanofluid electrolytes for aqueous flow batteries: the mechanism of nanoparticles as catalysts for redox reactions. J. Energy Storage 38, 102529.
Kundu, S., Bramhaiah, K., Bhattacharyya, S., 2020. Carbon-based nanomaterials: in the quest of alternative metal-free photocatalysts for solar water splitting. Nanoscale Adv. 2 (11), 5130–5151.
Léon, A. (Ed.), 2008. Hydrogen Technology: Mobile and Portable Applications. Springer Science & Business Media.
Leong, Y.K., Ong, B.C., 2003. Critical zeta potential and the Hamaker constant of oxides in water. Powder Technol. 134 (3), 249–254.
Li, X., Chen, W., Zou, C., 2020. An experimental study on β-cyclodextrin modified carbon nanotubes nanofluids for the direct absorption solar collector (DASC): specific heat capacity and photo-thermal conversion performance. Sol. Energy Mater. Sol. Cell. 204, 110240.
Li, W., Tian, H., Ma, L., Wang, Y., Liu, X., Gao, X., 2022. Low-temperature water electrolysis: fundamentals, progress, and new strategies. Materials Advances 3 (14), 5598–5644.
Liu, C., Lee, H., Chang, Y.H., Feng, S.P., 2016. The study of electrical conductivity and diffusion behavior of water-based and ferro/ferricyanide-electrolyte-based alumina nanofluids. J. Colloid Interface Sci. 469, 17–24.
Lohmann-Richters, F.P., Renz, S., Lehnert, W., Müller, M., Carmo, M., 2021. Challenges and opportunities for increased current density in alkaline electrolysis by increasing the operating temperature. J. Electrochem. Soc. 168 (11), 114501.
Matsushima, H., Iida, T., Fukunaka, Y., 2012. Observation of bubble layer formed on hydrogen and oxygen gas-evolving electrode in a magnetic field. J. Solid State Electrochem. 16, 617–623.
Maxwell, J.C., 1873. A Treatise on Electricity and Magnetism, vol. 1. Clarendon Press, Oxford.
Minea, A.A., 2019. A review on electrical conductivity of nanoparticle-enhanced fluids. Nanomaterials 9 (11), 1592.
Nie, J., Chen, Y., Boehm, R.F., Katukota, S., 2008. A photoelectrochemical model of proton exchange water electrolysis for hydrogen production. J. Heat Tran. 130 (4).
Ohshima, H., 2003. Electrokinetic phenomena in a dilute suspension of spherical colloidal particles in a salt-free medium. Colloids Surf. A Physicochem. Eng. Asp. 222 (1–3), 207–211.
Prasher, R., 2005. Brownian-motion-based convective-conductive model for the thermal conductivity of nanofluids. In: Heat Transfer Summer Conference, vol. 47314, pp. 343–353.
Prasher, R., Phelan, P.E., Bhattacharya, P., 2006. Effect of aggregation kinetics on the thermal conductivity of nanoscale colloidal solutions (nanofluid). Nano Lett. 6 (7), 1529–1534.
Rasool, M.A., Sattar, R., Anum, A., Al-Hussain, S.A., Ahmad, S., Irfan, A., Zaki, M.E., 2023. An insight into carbon nanomaterial-based photocatalytic water splitting for green hydrogen production. Catalysts 13 (1), 66.
Rausch, B., Symes, M.D., Chisholm, G., Cronin, L., 2014. Decoupled catalytic hydrogen evolution from a molecular metal oxide redox mediator in water splitting. Science 345 (6202), 1326–1330.
Said, Z., Sundar, L.S., Tiwari, A.K., Ali, H.M., Sheikholeslami, M., Bellos, E., Babar, H., 2022. Recent advances on the fundamental physical phenomena behind stability, dynamic motion, thermophysical properties, heat transport, applications, and challenges of nanofluids. Phys. Rep. 946, 1–94.
Schalenbach, M., Tjarks, G., Carmo, M., Lueke, W., Mueller, M., Stolten, D., 2016. Acidic or alkaline? Towards a new perspective on the efficiency of water electrolysis. J. Electrochem. Soc. 163 (11), F3197.
Sharaf, O.Z., Taylor, R.A., Abu-Nada, E., 2020. On the colloidal and chemical stability of solar nanofluids: from nanoscale interactions to recent advances. Phys. Rep. 867, 1–84.
Sheikholeslami, M., Bhatti, M.M., 2017. Active method for nanofluid heat transfer enhancement by means of EHD. Int. J. Heat Mass Tran. 109, 115–122.
Shen, L.P., Wang, H., Dong, M., Ma, Z.C., Wang, H.B., 2012. Solvothermal synthesis and electrical conductivity model for the zinc oxide-insulated oil nanofluid. Phys. Lett. 376 (10–11), 1053–1057.
Stamenkovic, V.R., Strmcnik, D., Lopes, P.P., Markovic, N.M., 2017. Energy and fuels from electrochemical interfaces. Nat. Mater. 16 (1), 57–69.
Sudhaik, A., Raizada, P., Shandilya, P., Jeong, D.Y., Lim, J.H., Singh, P., 2018. Review on fabrication of graphitic carbon nitride based efficient nanocomposites for photodegradation of aqueous phase organic pollutants. J. Ind. Eng. Chem. 67, 28–51.
Taylor, R., Coulombe, S., Otanicar, T., Phelan, P., Gunawan, A., Lv, W., Rosengarten, G., Prasher, R., Tyagi, H., 2013. Small particles, big impacts: a review of the diverse applications of nanofluids. J. Appl. Phys. 113 (1), 1.
Teh, E.J., Leong, Y.K., Liu, Y., Ong, B.C., Berndt, C.C., Chen, S.B., 2010. Yield stress and zeta potential of washed and highly spherical oxide dispersions—critical zeta potential and Hamaker constant. Powder Technol. 198 (1), 114–119.
Timofeeva, E.V., Moravek, M.R., Singh, D., 2011. Improving the heat transfer efficiency of synthetic oil with silica nanoparticles. J. Colloid Interface Sci. 364 (1), 71–79.
Ulset, E.T., Kosinski, P., Zabednova, Y., Zhdaneev, O.V., Struchalin, P.G., Balakin, B.V., 2018. Photothermal boiling in aqueous nanofluids. Nano Energy 50, 339–346.
Waite, T.D., Cleaver, J.K., Beattie, J.K., 2001. Aggregation kinetics and fractal structure of γ-alumina assemblages. J. Colloid Interface Sci. 241 (2), 333–339.
Wang, R.T., Wang, J.C., 2016. Alumina nanofluids as electrolytes comparisons to various neutral aqueous solutions inside battery. Journal of Mechanics 32 (3), 369–379.
Wang, M., Wang, Z., Gong, X., Guo, Z., 2014. The intensification technologies to water electrolysis for hydrogen production–A review. Renew. Sustain. Energy Rev. 29, 573–588.
Wang, G., Zhang, Z., Wang, R., Zhu, Z., 2020. A review on heat transfer of nanofluids by applied electric field or magnetic field. Nanomaterials 10 (12), 2386.
Wei, S., Hikmati, J., Balakin, B.V., Kosinski, P., 2022. Experimental study of hydrogen production using electrolyte nanofluids with a simulated light source. Int. J. Hydrogen Energy 47 (12), 7522–7534.
Zawrah, M.F., Khattab, R.M., Girgis, L.G., El Daidamony, H., Abdel Aziz, R.E., 2016. Stability and electrical conductivity of water-base Al2O3 nanofluids for different applications. HBRC journal 12 (3), 227–234.
Zuccaro, L., Krieg, J., Desideri, A., Kern, K., Balasubramanian, K., 2015. Tuning the isoelectric point of graphene by electrochemical functionalization. Sci. Rep. 5 (1), 1–13.